ornl

OAK RIDGE NATIONAL LABORATORY

UNION CARBIDE

NUREG/CR-2299, Vol. 3
ORNL/TM-8149

LMFBR Aerosol Release and Transport Program Quarterly Progress Report for July-September 1981

T. S. Kress M. L. Tobias

Prepared for the U.S. Nuclear Regulatory Commission
Office of Nuclear Regulatory Research
Under Interagency Agreements DOE 40-551-75 and 40-552-75

OPERATED BY
UNION CARBIDE CORPORATION
FOR THE UNITED STATES
DEPARTMENT OF ENERGY

8205060131 820228
PDR NUREG
CR-2299 R PDR

Printed in the United States of America. Available from
National Technical Information Service
U.S. Department of Commerce
5285 Port Royal Road, Springfield, Virginia 22161

Available from

GPO Sales Program
Division of Technical Information and Document Control
U.S. Nuclear Regulatory Commission
Washington, D.C. 20555

This report was prepared as an account of work sponsored by an agency of the United States Government. Neither the United States Government nor any agency thereof, nor any of their employees, makes any warranty, express or implied, or assumes any legal liability or responsibility for the accuracy, completeness, or usefulness of any information, apparatus, product, or process disclosed, or represents that its use would not infringe privately owned rights. Reference herein to any specific commercial product, process, or service by trade name, trademark, manufacturer, or otherwise, does not necessarily constitute or imply its endorsement, recommendation, or favoring by the United States Government or any agency thereof. The views and opinions of authors expressed herein do not necessarily state or reflect those of the United States Government or any agency thereof.

NUREG/CR-2299, Vol. 3
ORNL/TM-8149
Dist. Category R7

Contract No. W-7405-eng-26

Engineering Technology Division

LMFBR AEROSOL RELEASE AND TRANSPORT PROGRAM QUARTERLY PROGRESS REPORT FOR JULY–SEPTEMBER 1981

T. S. Kress M. L. Tobias

Manuscript Completed – December 18, 1981
Date Published – January 1982

NOTICE This document contains information of a preliminary nature. It is subject to revision or correction and therefore does not represent a final report.

Prepared for the
U.S. Nuclear Regulatory Commission
Office of Nuclear Regulatory Research
Under Interagency Agreements DOE 40-551-75 and 40-552-75

NRC FIN No. B0121

Prepared by the
OAK RIDGE NATIONAL LABORATORY
Oak Ridge, Tennessee 37830
operated by
UNION CARBIDE CORPORATION
for the
DEPARTMENT OF ENERGY

CONTENTS

	Page
FOREWORD	v
SUMMARY	vii
GLOSSARY OF ACRONYMS	ix
ABSTRACT	1
1. INTRODUCTION	1
2. EXPERIMENTAL PROGRAM	3
2.1 Source Term Experiments in FAST/CRI-III	3
2.1.1 Introduction	3
2.1.2 Progress in FAST Facility modification for under-sodium tests	3
2.1.3 Progress in development of a revised under-sodium test plan	4
2.1.4 Progress in interpretation of ORNL-Sandia normalization test results	4
2.2 Secondary Containment Aerosol Studies in the NSPP	4
2.2.1 Introduction	4
2.2.2 LWR aerosol experiment No. 404	5
2.2.3 LWR aerosol experiment No. 405	8
2.3 Basic Aerosol Experiments in CRI-II	11
2.3.1 Introduction	11
2.3.2 Characterization of the oxide aerosols of silicon and boron	11
2.3.3 Silicon oxide and boron oxide aerosol morphology	13
2.4 Core-Melt Aerosol Release and Transport	18
2.4.1 Introduction	18
2.4.2 Interaction of PWR control rod molten-silver alloy with Zircaloy fuel cladding	19
2.4.3 Conclusions from melting experiments	21
2.4.4 Preliminary concept for a full 10-kg core-melt experimental facility	23
3. ANALYTICAL PROGRAM	24
3.1 Status of Analysis of Water Tests – Development of Improved Models	24
3.2 Linearized Modeling of Adiabatic Oscillations	26
3.2.1 Introduction and derivations	26
3.2.2 Comparison of linearized theory with experiment and with nonlinear calculations	29
3.3 Application of the UVABUBL Code to FAST	32
REFERENCES	33

FOREWORD

This report summarizes progress under the Aerosol Release and Transport (ART) Program [sponsored by the Division of Reactor Safety Research of the Nuclear Regulatory Commission (NRC)] for the period July–September 1981.

Work on this program was initially reported as Volume III of a four-volume series entitled *Quarterly Progress Report on Reactor Safety Programs Sponsored by the NRC Division of Reactor Safety Research*. Prior reports of this series are

Report No.	Period covered
ORNL/TM-4655	April–June 1974
ORNL/TM-4729	July–September 1974
ORNL/TM-4805	October–December 1974
ORNL/TM-4914	January–March 1975
ORNL/TM-5021	April–June 1975

Beginning with the report covering the period July–September 1975, work under this program is now being reported as *LMFBR Aerosol Release and Transport Program Quarterly Progress Report*. Prior reports under this title are

Report No.	Period covered
ORNL/NUREG/TM-8	July–September 1975
ORNL/NUREG/TM-9	October–December 1975
ORNL/NUREG/TM-35	January–March 1976
ORNL/NUREG/TM-59	April–June 1976
ORNL/NUREG/TM-75	July–September 1976
ORNL/NUREG/TM-90	October–December 1976
ORNL/NUREG/TM-113	January–March 1977
ORNL/NUREG/TM-142	April–June 1977
ORNL/NUREG/TM-173	July–September 1977
ORNL/NUREG/TM-193	October–December 1977
ORNL/NUREG/TM-213	January–March 1978
ORNL/NUREG/TM-244	April–June 1978
ORNL/NUREG/TM-276	July–September 1978
ORNL/NUREG/TM-318	October–December 1978
ORNL/NUREG/TM-329	January–March 1979
ORNL/NUREG/TM-354	April–June 1979
ORNL/NUREG/TM-376	July–September 1979
ORNL/NUREG/TM-391	October–December 1979
ORNL/NUREG/TM-416	January–March 1980
ORNL/NUREG/TM-417	April–June 1980
ORNL/TM-7806	July–September 1980
ORNL/TM-7884	October–December 1980
ORNL/TM-7946	January–March 1981
ORNL/TM-7974	April–June 1981

Copies of all these reports are available from the Technical Information Center, Oak Ridge, Tennessee 37830.

SUMMARY

M. L. Tobias

The Aerosol Release and Transport Program at Oak Ridge National Laboratory (ORNL) is designed to investigate the release, transport, and behavior of radionuclides originating from a severe accident resulting in core melting. Aspects of the program apply to both light-water reactors (LWR) and liquid-metal fast breeder reactors. The experimental programs are being conducted in the Fuel Aerosol Simulant Test (FAST) Facility [which also includes the Containment Research Installation-III (CRI-III) vessel], the Nuclear Safety Pilot Plant (NSPP) Facility, and the CRI-II Facility. The analytical efforts are designed to support the experiments and to provide an independent assessment of the safety margins that exist for the estimation of the radiological consequences of a core meltdown accident.

During this quarter, the major effort in the FAST/CRI-III experimental program was preparation for under-sodium tests. Analysis of under-water test data continued, as did the development of a revised under-sodium test plan. Calculations using the UVABUBL code were performed in this connection for both water and sodium FAST test conditions. Work continued in ORNL-Sandia normalization experiment interpretation.

Two tests were performed in the NSPP to study U_3O_8 aerosol behavior in steam-air environments that might typify LWR accident conditions. Particular attention was given to improvement of mixing conditions in the test vessel to eliminate concentration gradients observed in three earlier tests. In one of the tests reported here, the aerosol was generated into a steam-air atmosphere. In the other, the U_3O_8 was introduced into a dry atmosphere, and steam was injected 42 min after terminating aerosol generation. Condensing steam was again effective in removing aerosol from the closed volume of the NSPP. (More studies will have to be done to determine whether this observation scales to LWR containments.)

In the program of basic experiments in CRI-II to simulate core-concrete interaction aerosols, SiO_2 and boric oxide aerosols were generated and subjected to size-distribution analysis using the Los Alamos National Laboratory-Stöber spiral centrifuge. The silicon dioxide aerosol was further characterized by surface-area measurements by the Brunauer-Emmet-Teller method, and the number of primary particles per agglomerate was estimated. This was found intermediate to those previously reported for U_3O_8 and Fe_2O_3.

Additional experiments in the core-melt aerosol studies program are reported. On the basis of these and previous tests, a tentative ranking of the mass fractions of various material types in a pressurized-water reactor type aerosol has been made. The experiments on the 0.5-kg facility continue to provide information for the design of a 10-kg facility.

In the analytical program, work on implementing the UVABUBL code continues. A notable problem with the code is its use of the "infinite sea" Rayleigh equation model. Results from a much simpler adiabatic "piston" model code show better agreement with experimental results. In particular, the piston model exhibits effects of depth and cover-gas pressure quite similar to those observed experimentally.

A linearization of the equations for the piston model was carried out. This analysis, while leading to less accurate values of the periods than obtainable from the nonlinear model because of the basic "small oscillation" assumption, is nevertheless found to afford a useful formulation of the way depth, fluid density, cover-gas pressure, and fuel mass vaporized affect the period. The linearized theory results are compared with those from the nonlinear model as well as with experimental results.

GLOSSARY OF ACRONYMS

ART	Aerosol Release and Transport
ACRR	Annular Core Research Reactor
AMMD	aerodynamic mass median diameter
BET	Brunauer-Emmet-Teller method
CDA	core-disruptive accident
CDV	capacitor discharge vaporization
CRI	Containment Research Installation
CSTF	Containment Systems Test Facility
CRBR	Clinch River Breeder Reactor
FAST	Fuel Aerosol Simulant Test
GSD	geometric standard deviation
HCDA	hypothetical core-disruptive accident
LANL	Los Alamos National Laboratory
LMFBR	Liquid-Metal Fast Breeder Reactor
LWR	Light-Water Reactor
NRC	Nuclear Regulatory Commission
NSPP	Nuclear Safety Pilot Plant
ORNL	Oak Ridge National Laboratory
PSL	polystyrene latex
PT	plasma torch
PWR	pressurized-water reactor
RF	radio frequency
SEM	scanning electron microscope
TEM	transmission electron microscope

LMFBR AEROSOL RELEASE AND TRANSPORT PROGRAM QUARTERLY PROGRESS REPORT FOR JULY–SEPTEMBER 1981

T. S. Kress M. L. Tobias

ABSTRACT

This report summarizes progress for the Aerosol Release and Transport Program sponsored by the Office of Nuclear Regulatory Research, Division of Accident Evaluation of the Nuclear Regulatory Commission for the period July–September 1981. Topics discussed include (1) preparations for under-sodium tests at the Fast Aerosol Simulant Test Facility, (2) progress in interpretation of Oak Ridge National Laboratory–Sandia Laboratory normalization test results, (3) U_3O_8 in steam (light-water reactor accident) aerosol experiments conducted in the Nuclear Safety Power Plant, (4) experiments on B_2O_3 and SiO_2 aerosols at the Containment Research Installation-II Facility, (5) fuel-melting tests in small-scale experimental facilities for the core-melt aerosol program, (6) analytical comparison of simple adiabatic nonlinear and linear analytical models of bubble oscillation phenomena with experimental data.

---

1. INTRODUCTION

The Aerosol Release and Transport (ART) Program at Oak Ridge National Laboratory (ORNL), sponsored by the Office of Nuclear Regulatory Research, Division of Accident Evaluation of the Nuclear Regulatory Commission, is a safety program concerned with radionuclide release and transport. The program's scope includes radionuclide release from fuel, transport to and release from primary containment boundaries, and behavior within containments. The overall goal of the program is to provide the analytical methods and experimental data necessary to assess the quantity and transient behavior of radionuclides released from reactor cores as a result of postulated events of varying severity up to and including accidents resulting in core melting.

The program is divided into several related experimental and analytical activities:

1. studies related to hypothetical liquid-metal fast breeder reactor (LMFBR) core-disruptive accidents (CDAs) that involve fuel interactions, expansion, and thermal behavior within the sodium pool as the resultant fuel-vapor bubble is produced and transported through the sodium to the cover-gas region;
2. development of apparatus to investigate the characteristics and transport behavior of materials vaporized from molten fuel;

3. study of the characteristics and behavior of fuel-simulant aerosols in several small vessels; and
4. production and study of aerosols in the Nuclear Safety Pilot Plant (NSPP) for the validation of models, with particular emphasis on the behavior of mixtures of nuclear aerosol species relevant to both light-water reactor (LWR) and LMFBR systems.

Varying levels of effort are anticipated within these categories with analytical models accompanying the experimental work. The analytical requirements fall into four categories: (1) fuel response to high rates of energy deposition, (2) fuel-bubble dynamic behavior and transport characteristics under sodium, (3) release of aerosols and fission products from heating and melting fuel, and (4) dynamic aerosol behavior at high concentrations in the bubble and containment atmospheres.

An attempt will be made to consolidate and present the analyses and data in a manner that will facilitate direct assessment of the radiological hazard associated with arbitrary hypothetical accident scenarios.

2. EXPERIMENTAL PROGRAM

2.1 Source-Term Experiments in FAST/CRI-III

A. L. Wright A. M. Smith
J. M. Rochelle

2.1.1 Introduction

The Fuel Aerosol Simulation Tests (FAST) and the Containment Research Installation-III (CRI-III) tests are performed by using the capacitor discharge vaporization (CDV) technique to place uranium dioxide fuel samples into the high-energy states that could be produced in LMFBR hypothetical CDAs. The primary goal of the FAST/CRI-III test program is to use the experimental results as a data base for developing analytical models that could be used to predict fuel transport through the coolant in severe accidents.

The major effort this quarter was related to preparing for under-sodium tests. This effort included test facility modification and preparation of a new work plan for the sodium tests. Additionally, analysis of underwater test results continued; some improvements to the test modeling will be discussed here and in Sect. 3.

Finally, a brief description of analysis efforts related to understanding Sandia normalization test results will be presented.

2.1.2 Progress in FAST Facility modification for under-sodium tests

Major progress in test facility modification occurred this quarter. However, because of the 7-week craft union strike, all modifications were not completed. Briefly, the following work was done:

1. Installation of heaters and thermocouples on the test vessel and the sodium fill system was completed. This included the installation of 24 additional thermocouples on the test vessel; these thermocouples will be tied directly to the PDP/8A data acquisition system.
2. Thermal insulation of the test vessel and sodium fill system was completed.
3. Modifications to the sample preheater to permit simultaneous vaporization of three samples were begun.
4. Checkout of the test facility instrumentation (such as thermocouples) was started.

Additionally, an internal Quality Assurance audit of the test facility was successfully completed in August of this quarter. The under-sodium tests are almost certain to begin early next quarter.

2.1.3 Progress in development of a revised under-sodium test plan

The UVABUBL code and simplified model codes described in Sect. 3 are being used to do calculations that will guide us in developing the new sodium test plan. Calculations being done – the results of which will be discussed in the test plan report – include:

1. UVABUBL calculations for water test conditions.
2. Scoping calculations, using UVABUBL and the simplified codes, and possible Clinch River Breeder Reactor (CRBR) vessel parameters and assumed CRBR core conditions at disassembly.
3. Scoping calculations, using UVABUBL and the simple models, for various possible [illegible] sodium test conditions. Of particular interest are calculations in which the bubble source is assumed to increase by a factor of 3, as will be done in the later multipin tests.

2.1.4 Progress in interpretation of ORNL-Sandia normalization test results

The ORNL-Sandia normalization experiments were described in a previous progress report.[2] In a number of the tests, a 0.635-cm (0.25-in.) length of UO_2 pellet was exposed, and photographic measurements were made to try to determine the exposed pellet temperature during preheat and capacitor discharge. This quarter, calculations were performed to try to interpret the exposed pellet temperatures in terms of the temperatures of the pellets surrounded by UO_2 microspheres. These calculations use computer models that were initially developed to calculate the heating of samples containing only pellets that were surrounded by microsphere packing. To date, application of these models to the exposed pellet heating has been unsuccessful; in particular, the calculations indicate that the center of the exposed pellet heats much too rapidly during capacitor discharge.

Additionally, the detailed particle-size data from the Sandia in-reactor test and from CDV 76 are being evaluated.

2.2 Secondary Containment Aerosol Studies in the NSPP

R. E. Adams

2.2.1 Introduction

Studies relating to the behavior of aerosols released under LWR accident conditions into secondary containment environments were continued this quarter. Five single-component aerosol tests involving U_3O_8 aerosol in steam environments have been conducted. Tests 401-403 have been reported previously;[2,3] results from Tests 404 and 405 are contained in this report.

2.2.2 LWR aerosol experiment No. 404

Mixing of the U_3O_8 aerosol within the steam-air atmosphere has not been as uniform as in previous U_3O_8 aerosol tests under dry conditions. During Runs 401-403, an aerosol concentration gradient existed early in each run with the higher concentration existing in the upper portion of the vessel. In an attempt to improve mixing, a small air-driven fan was installed near the bottom of the vessel with the air movement directed upward. Run 404 was intended to duplicate the conditions of Run 403 with this fan operated during preliminary steam injection and over the first hour following aerosol introduction. As in previous tests, steam was introduced into the NSPP vessel, which was at -0.062 MPa (gauge) to bring the vessel atmosphere to a temperature of about 383 K and a gauge pressure of 0.105 MPa. This process required about 1 h. At this point, the rate of steam injection was reduced and the accumulated steam condensate, which had collected in the vessel during heat-up, was removed to a holding tank. The U_3O_8 aerosol generation was then started, and introduction of the aerosol into this environment continued for 16.3 min. Steam injection at lower rates continued for a period of 6 h. During this period, the pressure and temperature peaked at 172 min with values of 0.149 MPa (gauge) and 390 K noted; at termination of steam injection, the values were 0.0845 MPa (gauge) and 375 K. Vessel cooldown continued for the next 18 h.

During the test, measurements were made of aerosol mass concentration, particle size, fallout and plateout rates, total fallout and plateout, vessel atmosphere temperature, temperature gradient near the vessel wall, pressure, moisture content, and steam condensation rate on the vessel wall.

Aerosol mass concentration. The maximum average U_3O_8 aerosol mass concentration measured was about 23 $\mu g/cm^3$, which is greater than that noted in Run 403 by a factor of more than two. Operation of the fan mixer seemed to improve the mixing of the steam and aerosol somewhat, but concentrations were still not as uniform as those observed in previous tests under dry conditions. The concentration gradient noted in the previous three steam tests was modified with aerosol concentrations occasionally greater in the lower region of the vessel than in the upper region. Figure 1 contains the results from seven aerosol mass samplers. Samplers 151 and 152 are located in the upper region of the vessel; sampler 153 is located about midplane of the vessel; and sampler 154 is located in the lower region of the vessel. Samplers 155, 156, and 157 penetrate the vessel wall at about the same elevation as sampler 153.

The influence that operation of the fan mixer had on aerosol behavior may be observed by comparing the results of Run 403 with those of Run 404 on a normalized aerosol mass basis. Figure 2 shows that during the first hour of Run 404, there is an early reduction in aerosol concentration compared with Run 403. This may be caused by fan operation enhancing agglomeration with resulting increased fallout or impaction on vessel surfaces. Another possible cause may be the higher initial concentration. This behavior of the aerosol was also reflected in increased aerosol fallout and plateout noted early in the run. After stopping the fan 62 min after the start of aerosol generation, the rate of removal of aerosol appears to be the same for both tests.

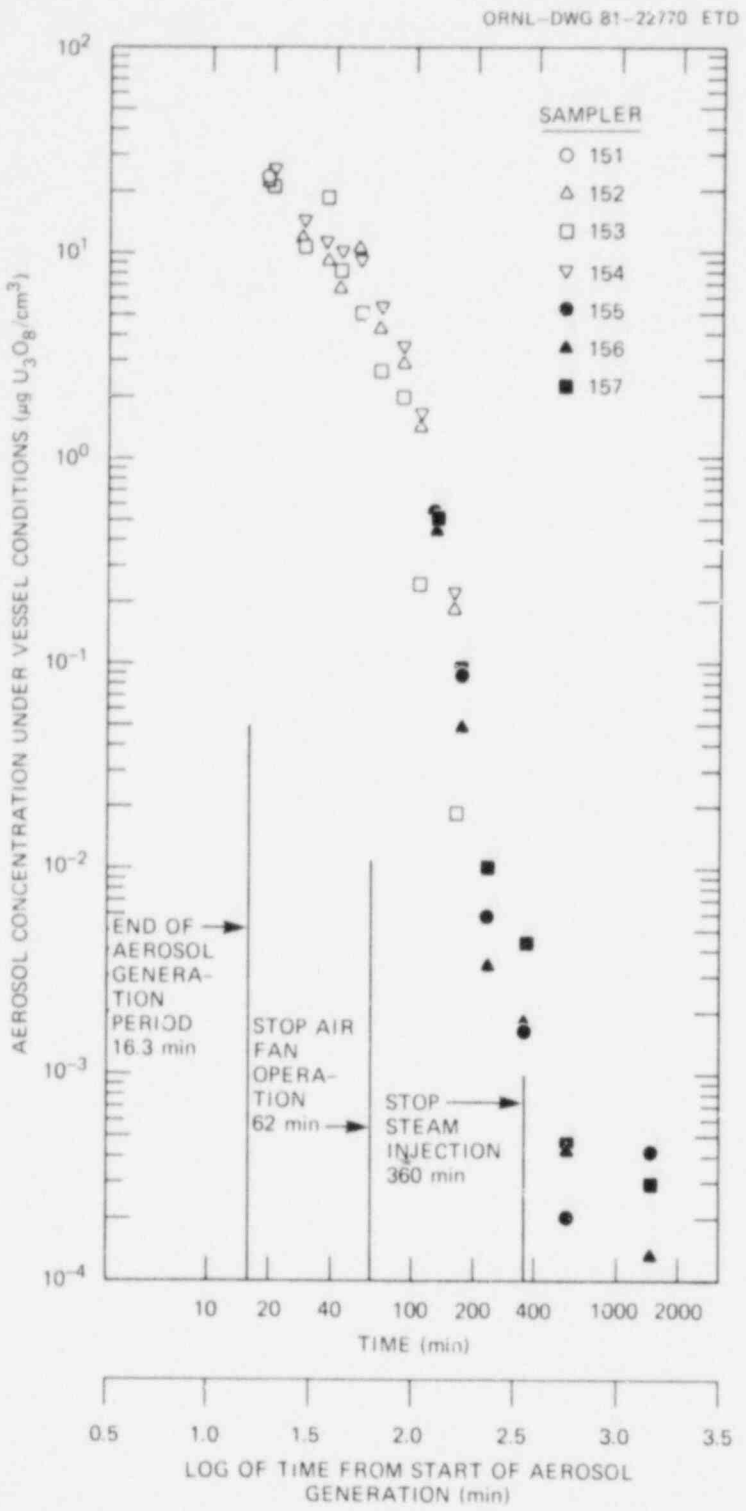

Fig. 1. Aerosol mass concentration as function of time for Run 404. Note that aerosol concentration is calculated under temperature and pressure that existed in vessel at time of sampling.

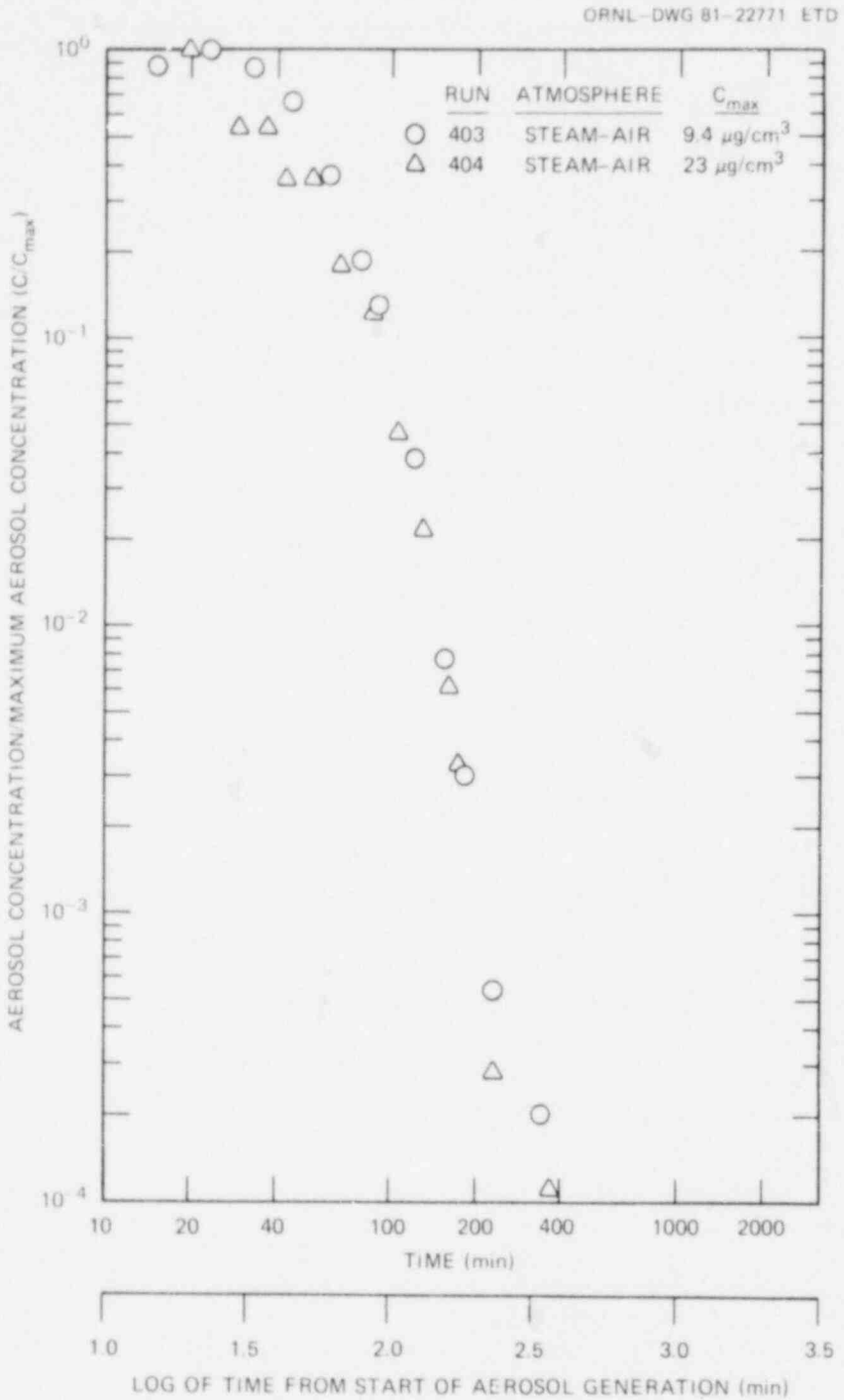

Fig. 2. Comparison of behavior of U_3O_8 aerosol in Run 403 and 404. Utilization of fan mixer in Run 404 may have caused early reduction in aerosol mass concentration.

Aerosol particle size. The aerodynamic mass median diameter (AMMD) of the U_3O_8 aerosol was measured both by the impactor and by the centrifuge sampler. The "wet" aerosol was dried by dilution with dry air prior to introduction into the samplers. The AMMD of the "dried" U_3O_8 aerosol ranged from about 1 to 2 μm over the first 3.4 h of the test. These values are comparable with those measured in the previous steam tests.

Aerosol distribution. At the termination of the test (24 h), the approximate aerosol distribution, as determined by the total fallout and total plateout samplers and the final filter sample, was as follows: aerosol settled onto the floor of the vessel, 63%; aerosol plated onto internal surface, 37%; and aerosol still suspended in vessel atmosphere, nil.

2.2.3 LWR aerosol experiment No. 405

The purpose of this test was to observe the influence of condensing steam on a previously agglomerated dry aerosol. The U_3O_8 aerosol was introduced over a period of 18 min into the NSPP vessel, which contained a dry atmosphere (relative humidity <20%) under ambient conditions of temperature and pressure. After allowing ~42 min (after termination of aerosol generation) for the dry aerosol to agglomerate and achieve larger particle sizes, steam injection into the vessel was initiated. At the start of steam injection, the vessel pressure and temperature were 0.0075 MPa (gauge) and 304 K, respectively; 35 min later, the steam injection rate was reduced, and values for pressure and temperature of 0.159 MPa (gauge) and 380 K were recorded. At 120 min after the start of steam injection, the steam flow was stopped, and values for pressure and temperature of 0.145 MPa (gauge) and 376 K were recorded. The vessel then entered a cooldown period of 21 h.

Aerosol mass concentration. An average maximum U_3O_8 aerosol mass concentration of 5.5 μg/cm³ was measured during the dry phase of the test. Operation of the fan mixer seems to have improved aerosol mixing during this dry phase. Results from all seven filter samplers are contained in Fig. 3.

Upon the start of steam injection into the vessel atmosphere and consequent rapid condensation of steam as the vessel started heat-up, an immediate reduction in aerosol mass concentration was noted. This aerosol behavior could be the result of (1) steam condensation onto the surface of the aerosol particles, with consequent fallout, and/or (2) a flux of steam toward the cooler inner surfaces of the vessel carrying aerosol particles that plate out. Figure 4 compares averaged aerosol concentration values for Run 405 with a comparable dry U_3O_8 aerosol test (Run 209).[4] Over the first 8 min of steam injection, the aerosol concentration was reduced by 88%; at termination of steam injection (2-h period), the concentration had been reduced by over 99%. In the absence of steam, Run 209 exhibited U_3O_8 aerosol concentration reduction of 20% and 82% over the same time intervals.

The results support the conclusion reached on the basis of the first 4 tests: for the NSPP, condensing steam is an effective agent for removing aerosol from a closed volume and appears, in these tests, to be the dominant factor in dictating the aerodynamic behavior of a U_3O_8 aerosol.

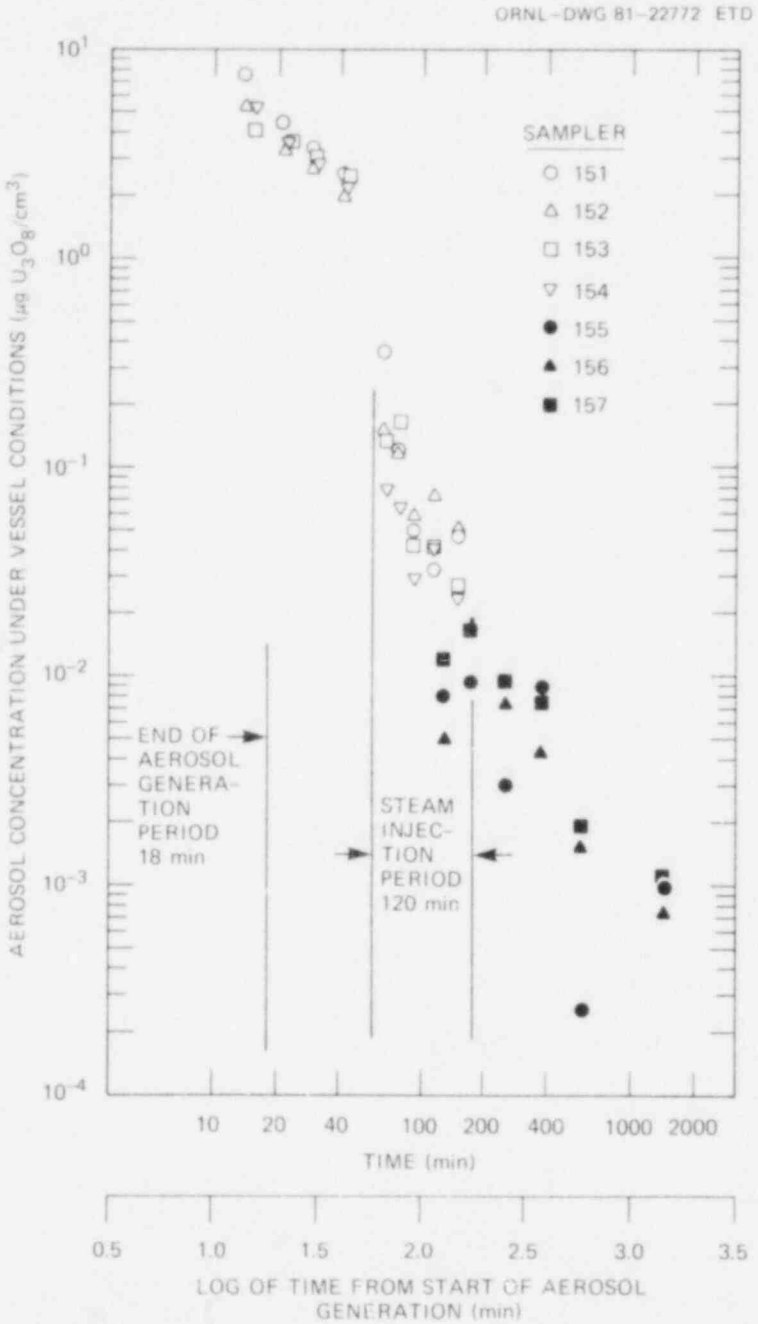

Fig. 3. Aerosol mass concentration as function of time for Run 405 illustrating the effect of steam injection on aerosol concentration. Note that aerosol concentration is calculated under temperature and pressure that existed in vessel at time of sampling.

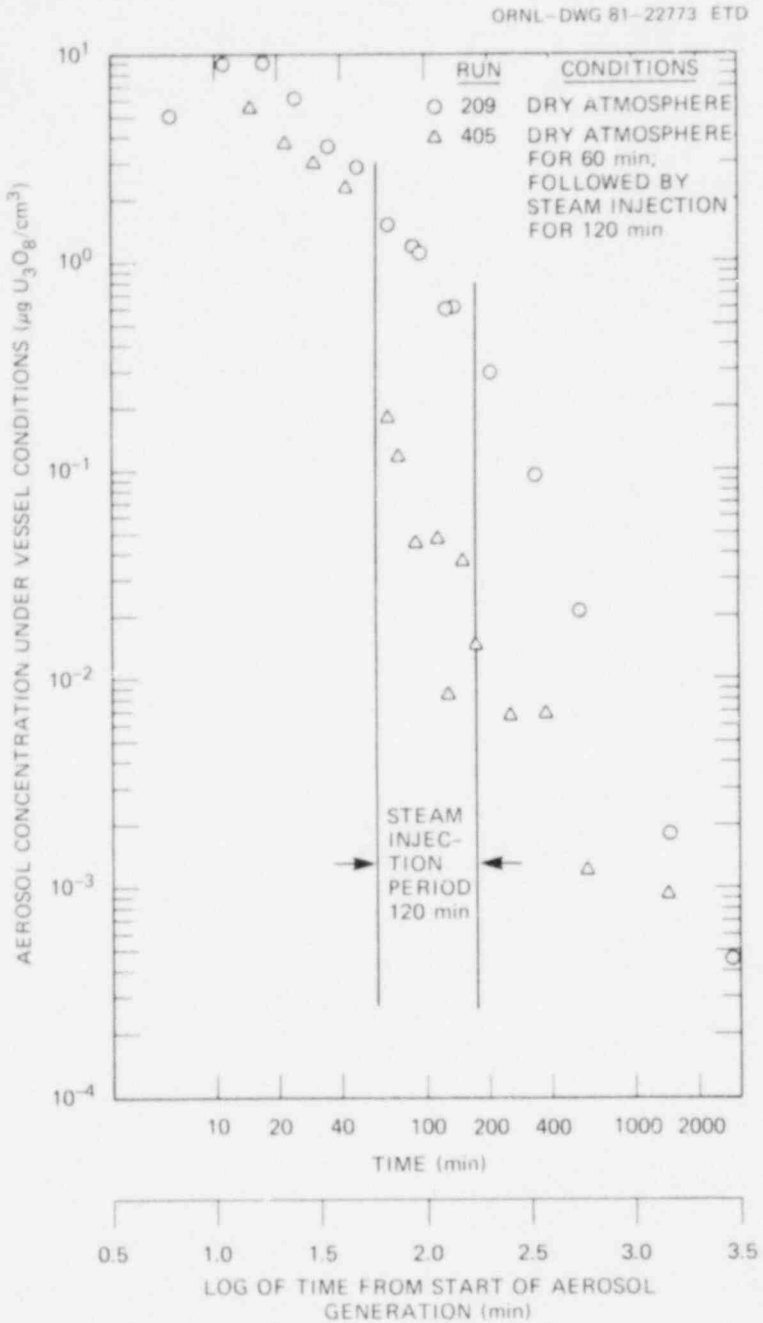

Fig. 4. Comparison of aerosol behavior in a dry atmosphere (Run 209) with that in a steam atmosphere (Run 405). Note rapid reduction in aerosol concentration (Run 405) upon start of steam injection.

More work will have to be done to determine whether this observation scales to LWR-size containments.

Aerosol particle size. Measurements both by the cascade impactor and the centrifuge sampler during the dry phase of the run gave values above 2 μm for the AMMD: 2.9 and 2.2 μm from the impactor and centrifuge, respectively. After introduction of steam, values of AMMD for the dried aerosol were measured by the impactor as 1.3 μm and by the centrifuge as 2 μm.

Aerosol distribution. At the termination of the run (24 h), the approximate aerosol distribution, as determined by the total fallout and plateout samplers and the final filter sample, was as follows: aerosol settled onto vessel floor, 74%; aerosol plated onto internal surfaces, 26%; and aerosol still suspended in vessel atmosphere, nil.

2.3 Basic Aerosol Experiments in CRI-II

G. W. Parker G. E. Creek
A. L. Sutton

2.3.1 Introduction

This program of basic experiments is carried out in the 5-m^3 test vessel, CRI-II, as part of the ART program. Vapor-condensation aerosols likely to comprise mixtures of importance in various nuclear accidents are systematically produced in 100-g quantities and then analyzed. Generation techniques are based on powder metal-oxygen combustion in a dc plasma arc or, in the case of sodium, by ignition of the liquid metal in a high-pressure spray.

In the program of basic aerosol experiments, there will be continuing investigations of the fundamental properties of the single-component oxides, including those of tin, iron or silver, cadmium, and indium for the pressurized-water reactor (PWR); boron for the boiling-water reactor; and calcium, aluminum, and silicon for the concrete interaction product for core meltdown.

A simplified summary of the systematics of size distribution and deposition rate of as many of these aerosols as possible should be a practical result of these experiments.

2.3.2 Characterization of the oxide aerosols of silicon and boron

In four separate experiments, duplicate runs of SiO_2 and B_2O_3 were conducted and the resulting aerosols subjected to agglomerate size-distribution analysis by means of the Los Alamos National Laboratory-Stöber spiral centrifuge. A transmission electron microscope (TEM) photomicrograph of the SiO_2 (Fig. 5) shows the presence of a series of quite spherical primary particles with a wide range in diameter. Mass concentrations achieved were between only 8 and 12 g/m^3, primarily because of the low density of the elemental powder and the relatively large volume of oxygen required to completely oxidize the powder. In only one case, however, was incomplete oxidation evident, and this was in the first boric oxide

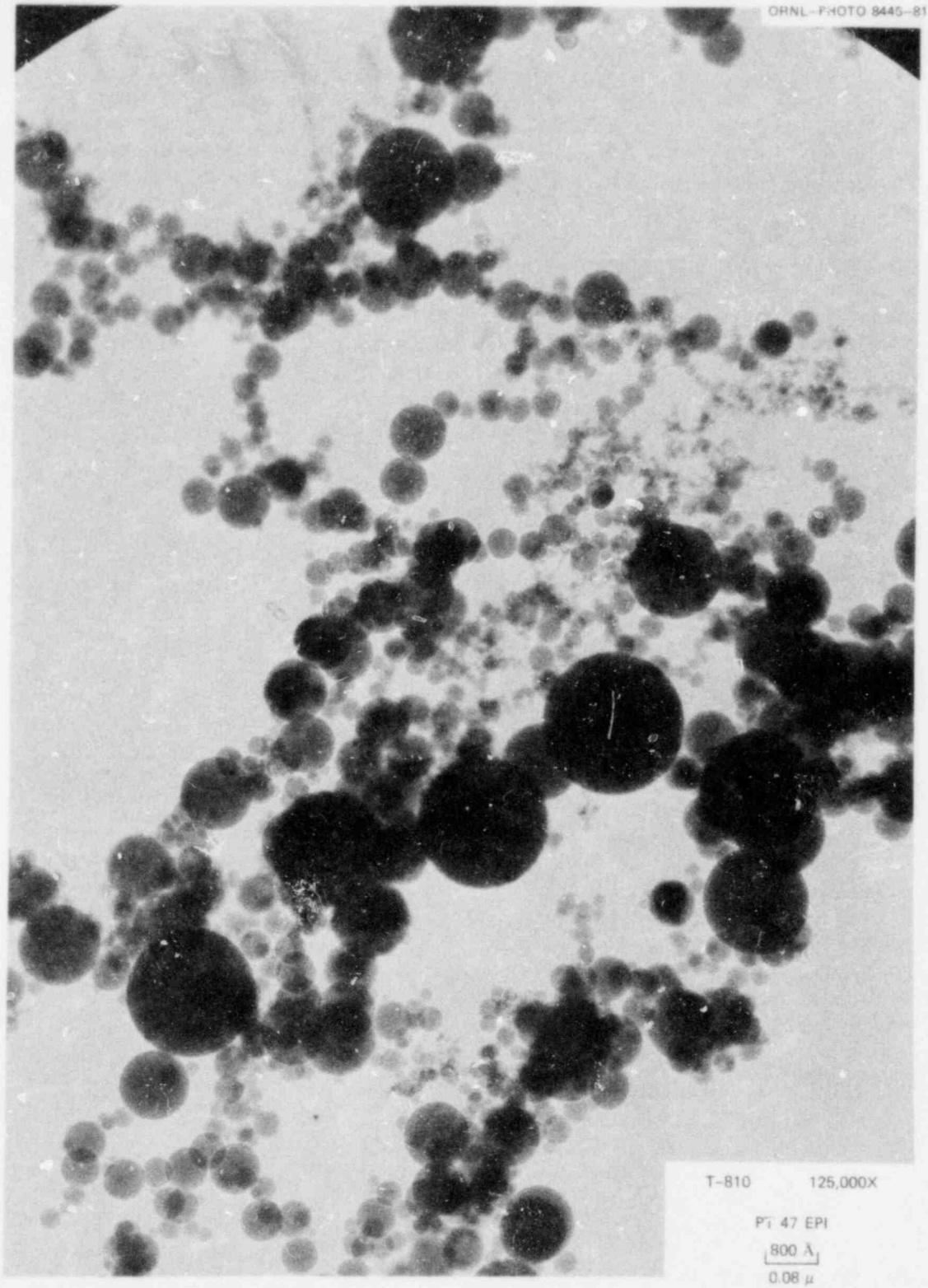

Fig. 5. Transmission photomicrograph of chain-agglomerate SiO_2 particles generated by the dc plasma metal-oxygen torch.

test (Run PT-49). Because the elemental boron and the oxide have about the same density (2.37 vs 2.46), little actual effect of the presence of boron in the oxide aerosol could be detected. Table 1 gives a summary of the results of the measurement of mass concentration, aerodynamic size, and geometric standard deviation (GSD). Figure 6(a and b) illustrates the similarity in appearance of the centrifuge size-distribution collection foils, and Figs. 7 and 8 show an approximate measure of the size distribution as a function of time using a correlation method of Smith and Jordan.[5] Here F = fraction of total aerosol in a sample; D_1, D_2 = maximum and minimum particle diameters contained in the sample; $\bar{D} = \sqrt{D_1 D_2}$; and $\Delta D = D_1 - D_2$. Further comparisons of the aerosol size measurements are plotted as a straight-line log-normal distribution in Figs. 9 and 10.

Additional experiments are planned in this series to include aluminum oxide, alone and in combination with calcium and silicon oxides as a simulant for core-concrete interaction aerosols.

Table 1. Aerosol characteristics in PT experiments 47-50

PT Run No.	Aerosol material	Maximum airborne concentration ($\mu g/cm^3$)	Agglomerate size AMMD[a] (μm)	Geometric standard deviation, σ
47	SiO_2	12.1	3.15	1.55
48	SiO_2[b]	10.4	3.33	1.52
49	B_2O_3	8.0	3.51	1.41
50	B_2O_3[c]	7.3	3.28	1.45

[a] Spiral centrifuge analysis.

[b] SiO_2 BET surface area = 38 m^2/g.

[c] B_2O_3 BET surface area = 35 m^2/g.

2.3.3 SiO_2 and B_2O_3 aerosol morphology

Molecular surface-area measurements by the Brunauer-Emmet-Teller (BET) method were used in each test to determine the approximate primary particle size. With the additional values of the actual number count of the individual agglomerates (for the SiO_2 only) as a function of time and

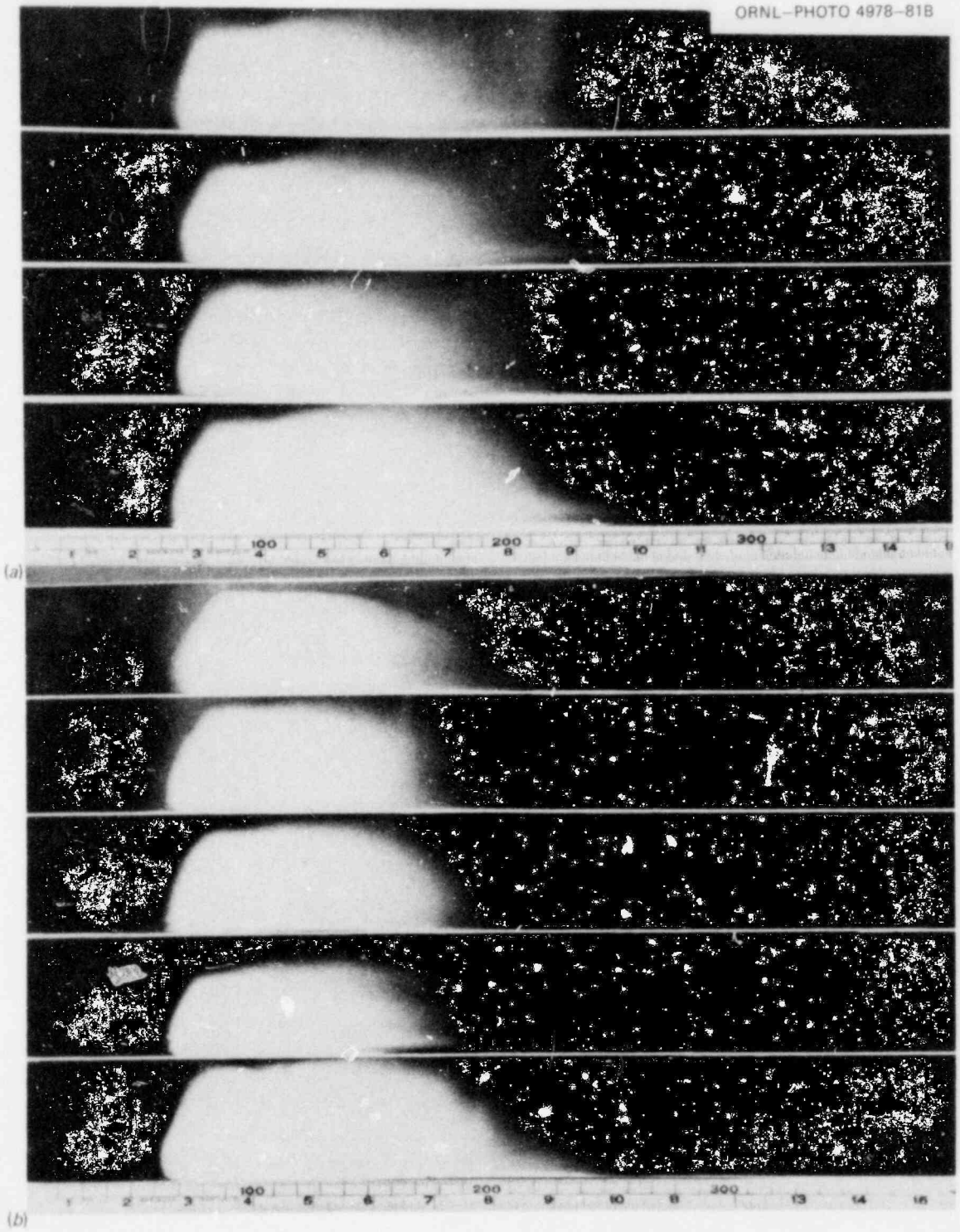

Fig. 6. Spiral centrifuge foils showing size distribution of aerosols of SiO_2 and B_2O_3 for (a) Run PT-49 and (b) Run PT-50.

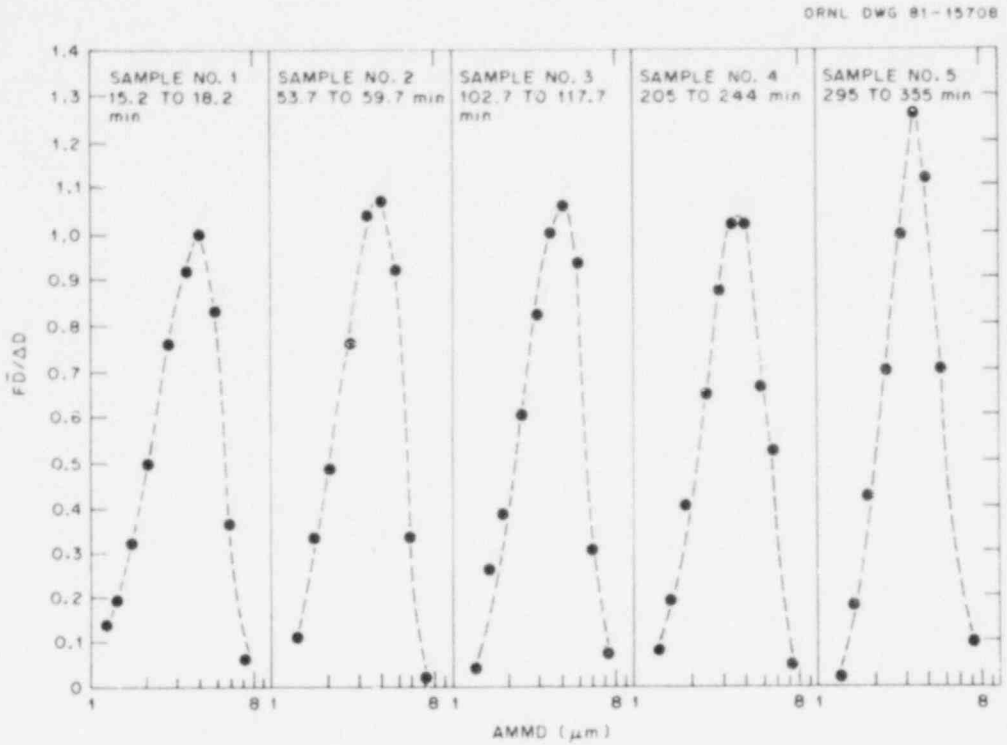

Fig. 7. Fractional distribution of SiO_2 aerosol particles showing relatively constant size distribution.

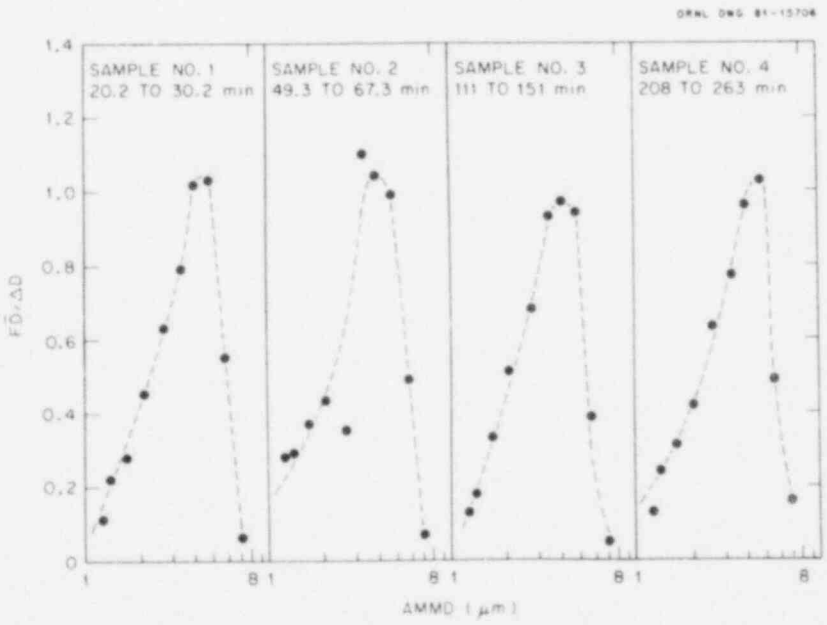

Fig. 8. Fractional distribution of B_2O_3 aerosol particles showing constant size distribution.

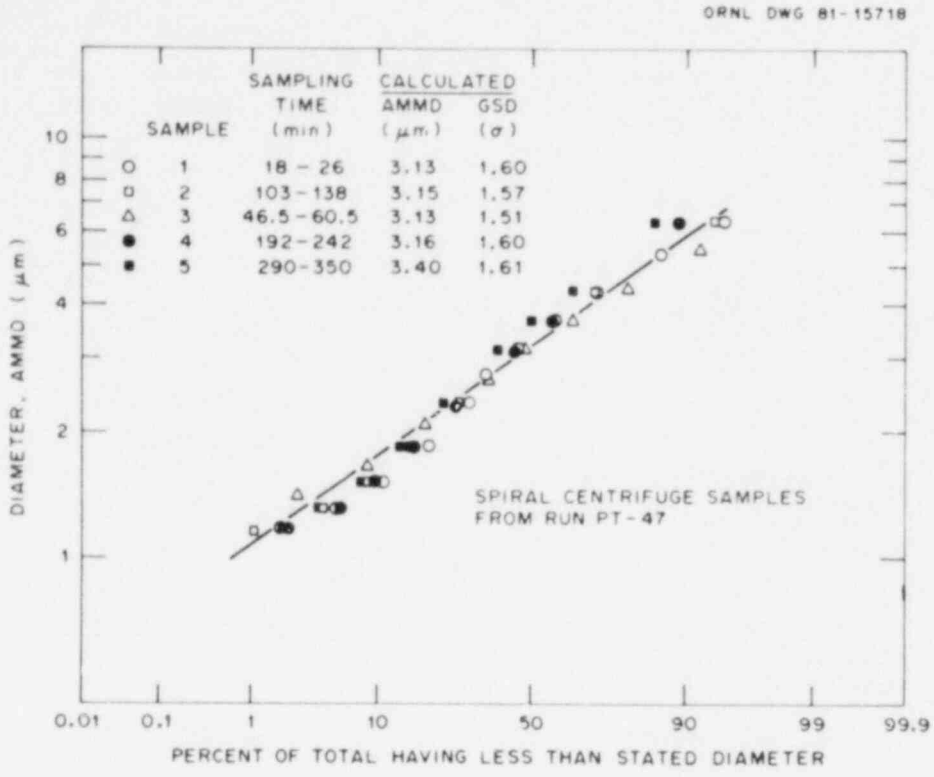

Fig. 9. SiO_2 aerosol AMMD and size distribution from Run PT-47.

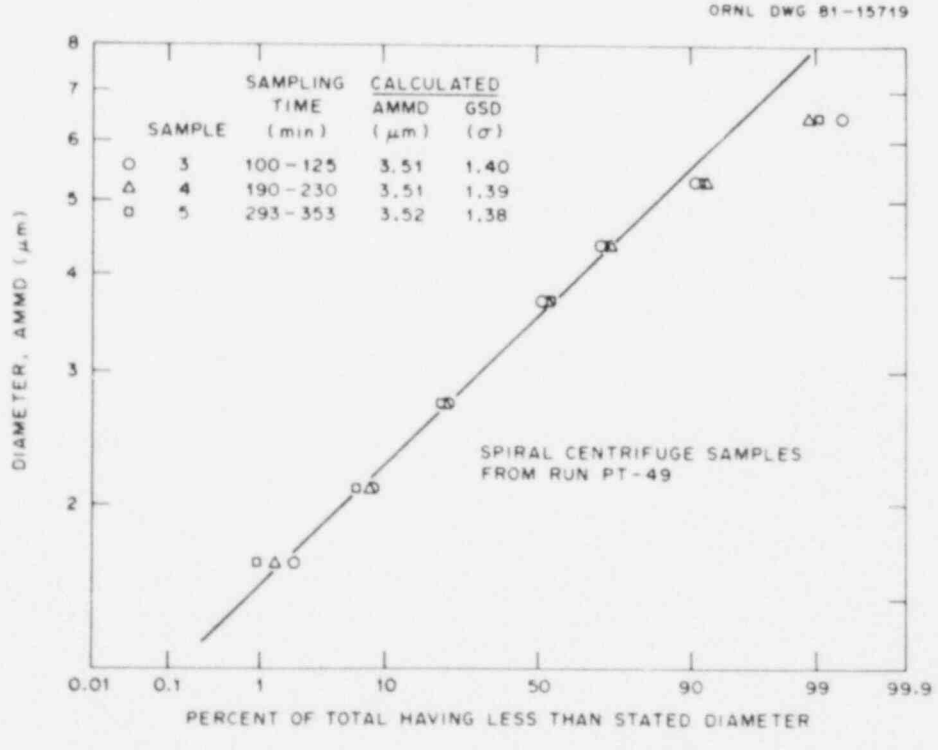

Fig. 10. B_2O_3 aerosol AMMD and size distribution from Run PT-49.

the airborne mass concentration, the approximate number of primary particles per agglomerate was determined. Because the nuclei counter being used will not count water-soluble aerosols, a different calculational method has to be used with B_2O_3.

The size of an average primary particle can be determined either by molecular surface area or by counting particles in a TEM photomicrograph. The surface-area method was required here because the resolution of the SiO_2 photomicrographs was not adequate for the extremely small microspheres.

Assuming a uniform size for primary particles, the following expression can be written in terms of the mass concentration C,

$$C = N_p \rho \frac{\pi D^3}{6} ,$$

where

N = number of agglomerated particles per cubic centimeter,
D = primary particle diameter,
ρ = particle density (g/cm^3),
C = concentration (g/cm^3).

Using a value of 8.25×10^{-6} cm for D (average from surface-area measurement) and 2.32 g/cm^3 for density (ρ) of SiO_2, we have

$$N_p = 1.47 \times 10^{15} C ,$$

and

$$N_t = 1.47 \times 10^{15} C/N_c ,$$

where

N_p = number of primary particles corresponding to concentration C,
N_c = number of nuclei (agglomerates) at concentration C,
N_t = average number of primary particles per agglomerate.

In the experiments, the observed value of N_c, which we denote by N_G, is obtained by use of the Gardner Nuclei Counter.

Results of the calculations (Table 2) show that the number of primary particles in an agglomerate is approximately an order of magnitude greater than those previously reported for U_3O_8 and about half of that reported for Fe_2O_3.

Table 2. Calculated number of primary particles in an average SiO_2 aerosol agglomerate

Time (min)	Airborne SiO_2 concentration (g/cm^3)	Nuclei/cm^3 observed, N_G	Primary particles per agglomerate, N_t
20	3.4×10^{-6}	3.06×10^5	1.63×10^4
40	1.9×10^{-6}	1.83×10^5	1.53×10^4
60	1.2×10^{-6}	1.25×10^5	1.41×10^4
80	0.78×10^{-6}	0.81×10^5	1.42×10^4
100	0.57×10^{-6}	0.58×10^5	1.44×10^4
150	0.36×10^{-6}	0.35×10^5	1.51×10^4
200	0.29×10^{-6}	0.28×10^5	1.52×10^4
250	0.25×10^{-6}	0.23×10^5	1.60×10^4

2.4 Core-Melt Aerosol Release and Transport

2.4.1 Introduction

The core-melt ART experiments are intended to address phenomena associated with LWR Class IX accidents, particularly the postulated large-scale vaporization of fission products, core components, and structural materials. To attain the desired high temperature and melting rates, the radio frequency (RF) induction melting of Zircaloy-clad fuel pins in presintered powdered oxide shells of UO_2 or ZrO_2, the "skull-melting" technique, has been chosen as the basis of the experimental system. A wide variety of core-simulating charge mixtures may be used in this method, and fission-product tracers may also be employed. Additionally, apparatus scaleup appears to be reasonably straightforward.

To simplify interpretation of the results of a parametric study of core-melt aerosol composition and behavior, we have elected to divide the matrix of the PWR experiments as follows:

1. Initial experiments with silver alloy (10 to 15% weight of the Zircaloy) at limited temperatures (below 1800°C), with and without excess steam, should reveal Ag, Cd, In, and stainless steel-Zircaloy interactions.
2. Secondary experiments without silver alloy and without stainless steel, to Zircaloy and eutectic melting temperatures (1800–2400°C), with and without steam, to measure tin release from Zircaloy.
3. Tertiary experiments without silver alloy and without tin (using zirconium cladding instead of Zircaloy) to the 2400°C eutectic melting temperature, to measure stainless steel component vaporization.
4. Initial fission-product simulant experiments without control rod alloys and without tin. These will include iodine and the semivolatiles Cs, Te, Sr, Ba, Sb, and Ru.

2.4.2 Interaction of PWR control rod molten-silver alloy with Zircaloy fuel cladding

The purpose of fuel-melt tests is to characterize and ultimately predict the behavior of core components at below eutectic melting temperatures. Localized melting is expected to be initially limited to the upper-center fuel regions, and varying amounts of molten silver and stainless steel should flow downward and solidify in cooler regions in contact with additional Zircaloy toward the bottom of the rods. Our large-scale (10-kg) experimental design will be capable of reproducing this postulated successive melt-and-freeze process through the addition of a mechanical elevator to follow the progress of the melt zone from the top to bottom of the core.

In several recent fuel-melt tests conducted at various limiting temperatures and furnace atmospheres, the apparent interaction of silver alloy with the Zircaloy cladding has led to extensive clad failure at relatively low temperatures below 1800°C, possibly near 1450°C, the melting point of stainless steel.

Our observations are consistent with the phase-diagram literature for silver and zirconium, which indicates that, with 10-mole % silver, zirconium forms an alloy that melts at a temperature lower than the melting point of stainless steel. Thus, silver melting and subsequent alloying can provide a potentially significant damage mechanism for cladding in some types of accidents.

In a previously reported experiment (Run CM-11), when pure silver was used as a substitute for the control Ag-In-Cd alloy, with incomplete melting, only silver aerosol was found in the vaporized solids. In a subsequent experiment (Run CM-12), when the silver was encased in stainless steel tubing, one of the minor stainless steel contituents, manganese, appeared in the aerosol to the extent of 5% of the silver. (Manganese is a minor constituent of some varieties of stainless steel.) In this experiment, incomplete melting was assured by the relatively low temperature (<1800°C) reached; however, extensive Zircaloy failure occurred, as shown in Fig. 11.

The next experimental variation introduced in this series was to mix the three components of the control rod alloy (Ag, In, and Cd) in the proper proportions and to encase the mixture in a stainless steel tube with a stainless-steel-simulated grid support arrangement on the fuel pins (Fig. 12) before heating to partial melting (~2000°C) with steam present. In this case, extensive alloy formation was evident between the silver mixture, the stainless steel, and the Zircaloy (Fig. 13). However, only cadmium was found in significant quantity in the vaporized aerosol. The vapor suppression effect of the metal mixture apparently inhibited the evaporation of silver, indium, and tin.

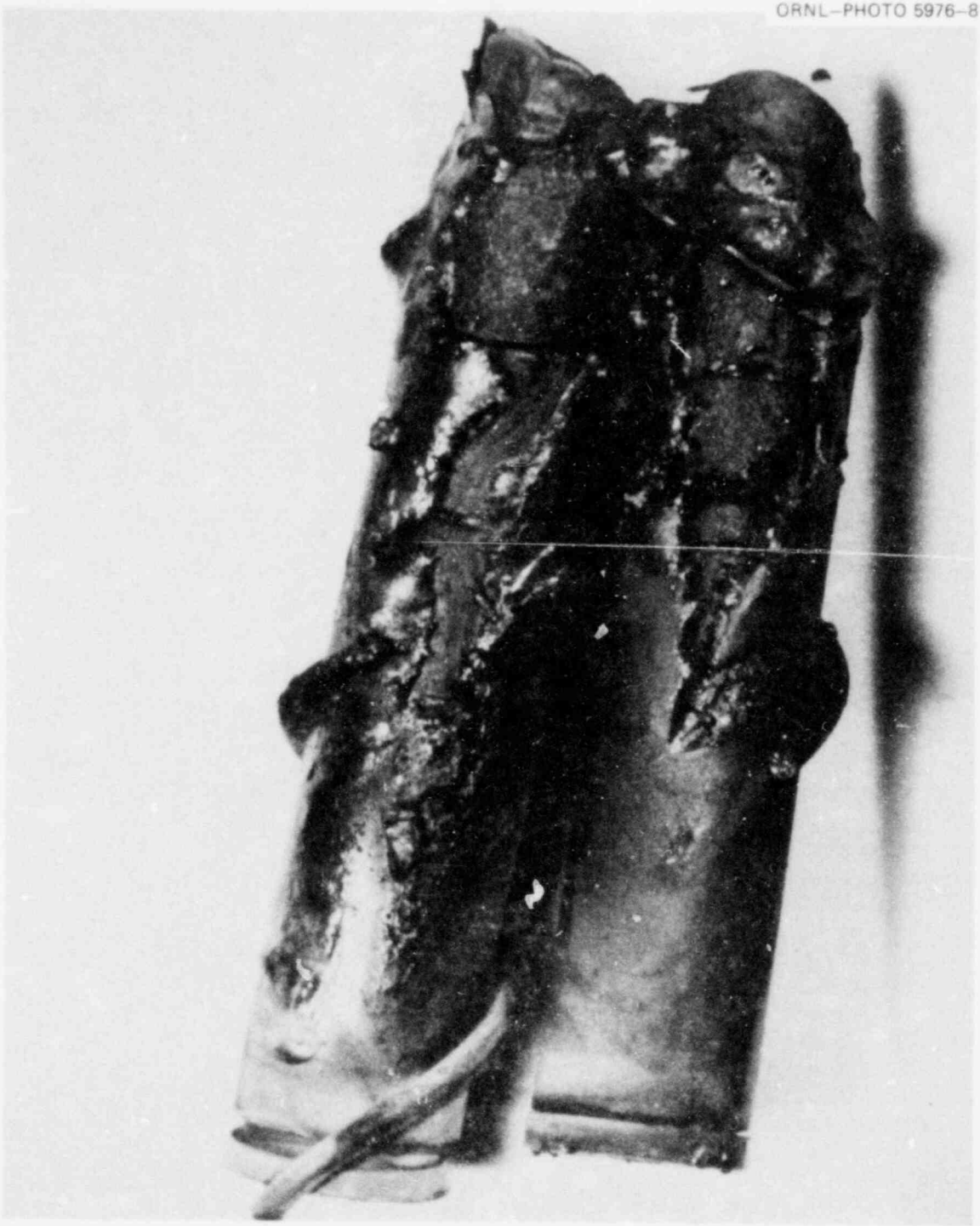

Fig. 11. Zircaloy clad failure induced by alloying with silver and stainless steel.

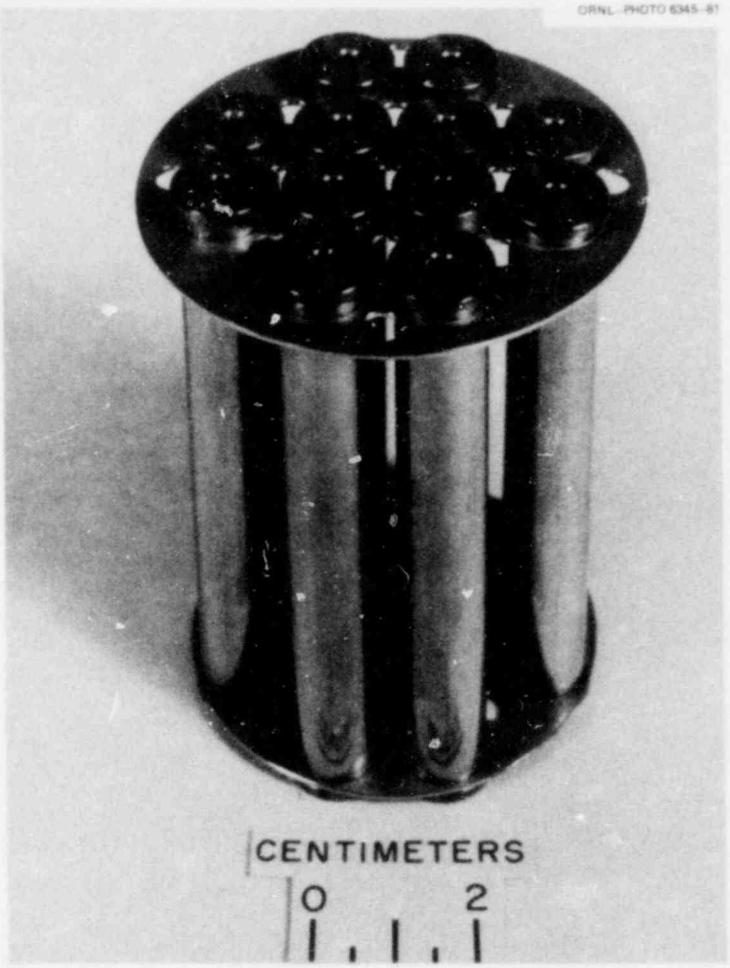

Fig. 12. Small test fuel bundle with stainless steel spacer-grid support sheets before heating.

2.4.3 Conclusions from melting experiments

The following preliminary conclusions on core-melt aerosol release phenomena seem to be consistent with the previously mentioned experiments:

1. Under the electric heat-driven conditions of the experiment, it would appear that control rod components (Ag, Cd, and In) would dominate initial PWR aerosol mass and probably contribute the largest fraction of aerosol; they have an appearance threshold temperature of ~1450°C. (More study will be needed to establish whether this would be true for the much more complex heat transfer conditions of a reactor accident.) Limiting the steam leads to excessive alloy formation between silver and Zircaloy and suppresses silver vaporization.
2. Fuel cladding (mainly tin) contributes the second largest fraction of aerosol mass. The appearance threshold temperature is 1850°C. With

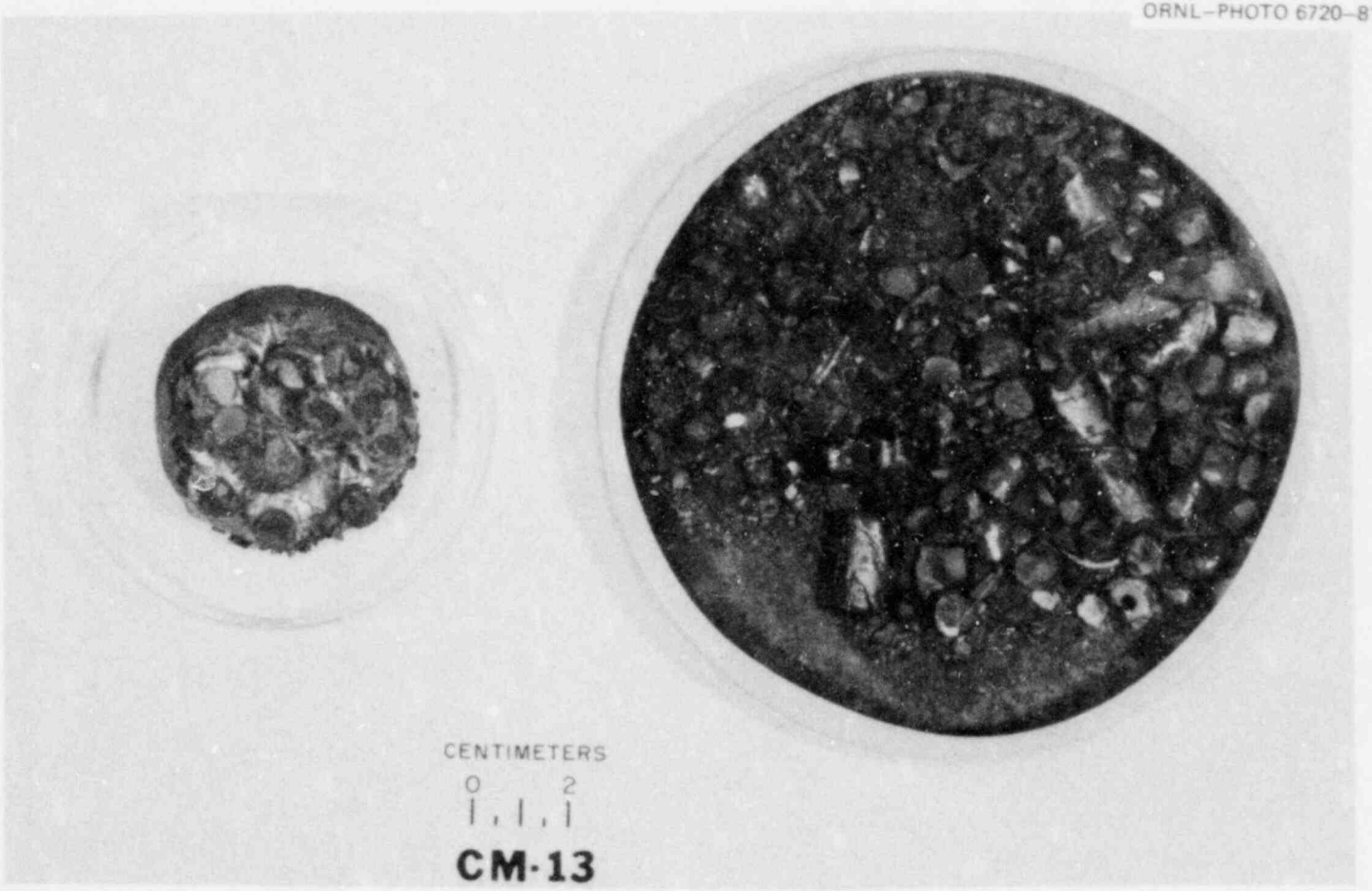

Fig. 13. Residues from core-melt experiment at 2200°C after the silver alloy and Zircaloy cladding melted into a single phase.

reduced steam and less Zircaloy oxidation, tin volatility is also suppressed.

3. Structural materials may contribute the third largest fraction of aerosol, primarily Mn, Fe, and FeO, from the stainless steel. The threshold temperature is ~2000°C.
4. Fission products should contribute the fourth largest fraction of aerosol mass. Appearance temperatures vary from 1300–2400°C, where the upper number is the limiting melt temperature at which the eutectic liquid ($Zr-ZrO_2-UO_2$) will flow downward to a cooler region.

2.4.4 Preliminary concept for a full 10-kg core-melt experimental facility

The past series of 0.5-kg scale experiments has served to illustrate some of the problem areas in the projected scaleup of the core-melt demonstration to 10 kg. These are being individually corrected in our future planning and include:

1. Addition of a heated upper-plenum stainless steel simulator to test primary system plateout.
2. Incorporation of an elevating lead screw that will permit partial melting in the middle and lower regions.
3. Substitution of a low-density ThO_2 crucible liner in the commercial stabilized zirconia crucible to resist melt-through. This is an in-house effort resulting from the nonavailability of commercial ThO_2-fabricated shapes.

The investigation of primary system plateout as an extension of the experiment is expected to have some input to the TRAP-MELT code development effort at Battelle Columbus Laboratories.

For an initial set of criteria to aid in the concept of the steam flow and surface parameters, we are referring to the existing data in WASH-1400, Appendix VII-H (Ref. 6) and NUREG-0772 (Ref. 7).

3. ANALYTICAL PROGRAM

M. L. Tobias A. L. Wright
W. P. Schuetz*

3.1 Status of Analysis of Water Tests – Development of Improved Models

A. L. Wright

As reported in a previous quarterly report,[8] the water test results are being analyzed using the UVABUBL code (developed by D. R. Bradley at the University of Virginia)[9]. This analysis indicated that UVABUBL could not yet predict results obtained for the bubble oscillation period; in particular, for most test conditions, predicted bubble periods were less than those measured.

The UVABUBL code includes detailed models for heat and mass transfer phenomena that could occur within the bubble. The code assumes that the expansion of the fuel-vapor source can be modeled by the Rayleigh constraint equation, which is:

$$\ddot{R} = \frac{(P_B - P_{CG})}{\rho R} - \frac{3}{2}\frac{\dot{R}^2}{R} , \qquad (1)$$

where

R = bubble radius,
P_B = bubble pressure,
P_{CG} = cover-gas pressure,
ρ = coolant density.

This equation describes the expansion and collapse of a bubble in an "infinite sea." However, in the FAST tests, the expansion of the bubble is constrained by the side walls of the vessel. Another way to model the expansion and collapse of the bubble is to assume that the motion of the liquid above the bubble is simply caused by the pressure difference between the bubble and the cover gas. In this model, the bubble pressure is assumed to be distributed evenly across the vessel cross section. The constraint equation using this "piston" model is:

$$\ddot{Z} = \frac{(P_B - P_{CG})}{\rho h} - g ,$$

---

*Research Participant, KfK, Karlsruhe.

where

Z = coordinate defining motion of liquid slug,
h = slug height, assumed to be the liquid height above the test sample,
g = acceleration of gravity.

Two simple computer codes were written, one using the Rayleigh constraint and the other using the piston constraint. In each code, it was assumed that no heat was lost from the bubble. Also, in each code, the internal bubble conditions (such as pressure and temperature) were determined using the same equations used in UVABUBL.

Table 3 presents a summary of bubble-period results, both measured and calculated, for various test parameters. These results show that, in general, the piston model does a much better job of calculating the test results. Of particular interest are results for varied liquid heights observed in conditions 2 and 3 in Table 3. In the tests and the piston model calculations, the bubble period increases with increasing liquid height. However, in the Rayleigh model calculations, the period decreases with increasing liquid height.

Based on these scoping calculations, UVABUBL is being modified so that both the Rayleigh and piston constraint models can be used.

Table 3. Measured and calculated[a] bubble-period results τ, for various FAST water test conditions

Test conditions for P_{CG}[b] (MPa)	Test conditions for L[c] (m)	τ_{FAST} (ms)	$\tau_{Rayleigh}$ (ms)	τ_{Piston} (ms)
2.02	1.12	5.3	3.75	4.75
0.122	0.20	36.7	35.0	39.0
0.122	1.12	51.4	29.0	69.0
0.025	1.12	173.9	48.0	144.0

[a] In the calculations it was assumed that the mass of fuel vaporized was 0.018 kg, the initial bubble temperature was 5000 K, the initial bubble radius was 0.0096 m, and no xenon gas was found in the bubble.

[b] P_{CD} = argon cover-gas pressure.

[c] L = water height above test sample.

3.2 Linearized Modeling of Adiabatic Oscillations

M. L. Tobias

3.2.1 Introduction and derivations

The analysis of vibrations of a slug of liquid oscillating between two gases (the piston model described in the previous section) can be linearized, leading to a closed-form relation for the period. This relation is sufficiently simple to permit the dependence of the period on the cover-gas pressure and the depth to be quantified. These relationships have been tested against the results obtained experimentally and with nonlinear calculations of the period obtained numerically.

In Fig. 14, V_1 represents the gas region produced by the CDV process, V_2 is the cover-gas region, and M is the mass of liquid above the CDV capsule. In this simple picture, we assume that the slug of liquid of weight Mg oscillates between the two volumes like a piston.

Assume adiabatic compression of both gases and assume that initially both gases have the same value of γ in the adiabatic expansion law,

$$PV^{\gamma} = \text{constant} . \tag{1}$$

We may write the following relationships:

$$P_1 V_1^{\gamma} = P_{10} V_{10}^{\gamma} , \tag{2}$$

$$V_1 = yA , \tag{3}$$

$$P_2 V_2^{\gamma} = P_{20} V_{20}^{\gamma} , \tag{4}$$

$$V_2 = (H - L - y)A , \tag{5}$$

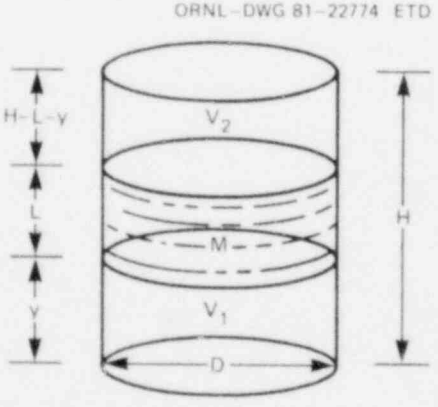

Fig. 14. Diagram of the "piston" model of bubble oscillation.

where P_{10}, P_{20}, V_{10}, and V_{20} are reference states for the upper and lower gas volumes.

By Newton's second law, we have (neglecting friction):

$$M\ddot{y} = -Mg - P_2A + P_1A \tag{6}$$

or

$$\ddot{y} = -g - \left(\frac{A}{M}\right) \frac{P_{20}V_{20}^{\gamma}}{[(H - L - y)A]^{\gamma}} + \left(\frac{A}{M}\right) \frac{P_{10}V_{10}^{\gamma}}{(Ay)^{\gamma}} \ . \tag{7}$$

To linearize this expression, assume that the vibration amplitude is small; that is, a small deviation δ about an equilibrium point $\bar{y}$ gives:

$$y = \bar{y} + \delta \ . \tag{8}$$

While this assumption is quite rough at best and leads to values of bubble periods that are not very accurate in absolute magnitude, relative relationships are discovered that are useful. Substituting (8) into (7) gives:

$$\ddot{\delta} = -g - \left(\frac{A}{M}\right) \frac{P_{20}V_{20}^{\gamma}}{(H - L - \bar{y} - \delta)^{\gamma}A^{\gamma}} + \left(\frac{A}{M}\right) \frac{P_{10}V_{10}^{\gamma}}{(\bar{y} + \delta)^{\gamma}A^{\gamma}} \ . \tag{9}$$

We define the equilibrium point $\bar{y}$ to be the point where $\ddot{\delta} = 0$ when $\delta = 0$, so we can obtain it from the relation:

$$0 = -g - \left(\frac{A}{M}\right) \frac{P_{20}V_{20}^{\gamma}}{[(H - L - y)A]^{\gamma}} + \left(\frac{A}{M}\right) \frac{P_{10}V_{10}^{\gamma}}{y^{\gamma}A^{\gamma}} \ , \tag{9a}$$

or

$$0 = -g - \left(\frac{A}{M}\right) \frac{P_{20}V_{20}^{\gamma}}{V_{2eq}^{\gamma}} + \left(\frac{A}{M}\right) \frac{P_{10}V_{10}^{\gamma}}{V_{1eq}^{\gamma}} \ , \tag{9b}$$

where V_{1eq} and V_{2eq} are defined as $A\bar{y}$ and $(H - L - \bar{y})A$, respectively.

Using a binomial theorem expansion to first order, that is, approximating $(K + \delta)^{-\gamma}$ as $K^{-\gamma}\,(1 - \gamma\delta/K)$, we obtain:

$$\ddot{\delta} = -\left[\left(\frac{A}{M}\right)\frac{P_{20}V_{20}{}^{\gamma}}{(H - L - \bar{y})^{\gamma}A^{\gamma}}\,\frac{\gamma}{H - L - \bar{y}} + \left(\frac{A}{M}\right)\frac{P_{10}V_{10}{}^{\gamma}}{A^{\gamma}\bar{y}^{\gamma}}\,\frac{\gamma}{\bar{y}}\right]\delta\ , \tag{10}$$

which is in the form of the familiar simple harmonic-motion equation.

Because $M = \rho LA$, where ρ is the liquid density, the period τ may be written:

$$\tau = \frac{2\pi}{\sqrt{\dfrac{\gamma}{\rho L}\left[P_{20}\left(\dfrac{V_{20}}{V_{2eq}}\right)^{\gamma}\left(\dfrac{1}{H - L - \bar{y}}\right) + P_{10}\left(\dfrac{V_{10}}{V_{1eq}}\right)^{\gamma}\dfrac{1}{\bar{y}}\right]}}\ . \tag{11}$$

The following simplifications, made on the basis of the dimensions and physical parameters of the FAST experiment, permit further insight. In Eq. (9), the value of g may be neglected in comparison with the other terms. Then $\bar{y}$ may be approximated as:

$$\bar{y} \cong [P_{10}/P_{20}]^{1/\gamma}\,[V_{10}/A]\ . \tag{12}$$

In Eq. (11) itself, if we were to take the reference values P_{10}, V_{10}, etc., as the equilibrium values, the expression would simplify to:

$$T \cong \frac{2\pi}{\sqrt{\dfrac{\gamma}{\rho L}\left(\dfrac{P_{2eq}}{H - L - \bar{y}} + \dfrac{P_{1eq}}{\bar{y}}\right)}}\ . \tag{13}$$

Observing that usually $\bar{y} \ll H - L$ and that $P_{1eq} \simeq P_{2eq} \simeq P$, the initial cover-gas pressure (the effect of g being relatively minor), the period may be expressed as

$$T \simeq \frac{2\pi}{\sqrt{\gamma P/(\rho L\bar{y})}}\ . \tag{14}$$

From Eq. (12), because P_{10} can be assumed proportional to the mass of fuel vaporized m_f, we have:

$$y = (\text{const.}) \times (m_f)^{1/\gamma} P^{-1/\gamma} . \tag{15}$$

Substituting in Eq. (14) with $\gamma = 1.67$ gives finally:

$$\tau = (\text{const.}) \times (\rho)^{1/2} L^{1/2} m_f^{0.3} P^{-0.8} , \tag{16}$$

or for arbitrary γ:

$$\tau = (\text{const.}) \times [\rho L (m_f)^{1/\gamma}]^{1/2} / [\gamma (\rho)^{\gamma+1/\gamma}]^{1/} \tag{16a}$$

3.2.2 Comparison of linearized theory with experiment and nonlinear calculations

The main equations of the linearized theory are embodied in Eqs. (11) and (16). The differential equation used in the nonlinear calculations is Eq. (7).

Several cases were run using a code that solved Eq. (7) numerically. The results are noted in the following tables in which some experimental results as well as linearized results from Eq. (11) are compared. The experimental results are taken from Table 3; the quantity of fuel actually vaporized in the experiments is not known.

The results in Table 4 on cover-gas pressure effects show that the correlation of the experimental data by $P^{-0.8}$ is satisfactory, even though the absolute values of the period produced by the linearized Eq. (11) disagree with the experiment by about a factor of 2. The nonlinear Eq. (7) gives far better agreement with the experiment. In Table 5 on fuel mass effect, the agreement between Eq. (11) and Eq. (7) is fairly good on a relative basis; nothing certain can be said about the experimental data that are included in the table for reference only. Table 6 (depth effect) again shows a fair agreement between the nonlinear Eq. (7) and the experiment, the predicted variation of period with depth seeming to hold. Table 7 compares the pressure variation of the periods computed by Eq. (7) with the predictions of Eq. (16) for various values of γ as well as with the experiment. Clearly agreement improves with larger values of γ. The results for the $\gamma = 1.0$ column show the effects of nonlinearity on the period, particularly at the lowest cover-gas pressure of 0.025 MPa. There, $\bar{y} \simeq 0.12$ m, so that the displacements are relatively large; moreover, the first term in the denominator of Eq. (13) cannot be neglected in comparison with the second. The change in period from 0.122 MPa to 0.025 MPa is thus strikingly small, but not at all in agreement with what is observed.

Equation (16) appears to be promising as a guide to scaling the period in terms of the experimental parameters.

Table 4. Effect of cover-gas pressure, P[a]

Cover-gas pressure (MPa)	Period (ms)		
	Linear theory, Eq. (11)	Nonlinear theory, Eq. (7)	Experiment
0.025	77 (3.3)[b]	128 (2.3)	173.9 (3.4)
0.122	23 (1.0)	55 (1.0)	51.4 (1.0)
0.202	15 (0.65)		
2.02	2.5 (0.11)	4.4 (0.08)	5.30 (0.10)

[a]Depth = 1.12 m, m_f = 10 g, γ = 5/3. Variation predicted by linear theory, Eq. (16): $\tau \sim P^{-0.3}$.

[b]Values in parentheses are ratios of periods in each column to those at P = 0.122 MPa.

Table 5. Effect of fuel mass, m_f[a]

Cover-gas pressure (MPa)	Fuel mass	Period (ms)		
		Linear theory, Eq. (11)	Nonlinear theory, Eq. (7)	Experiment
0.122	10	23 (1.0)[b]	55 (1.0)	51.4
0.122	5	19 (0.83)	45 (0.82)	
2.02	10	2.5 (1.0)	4.4 (1.0)	5.3
2.02	1	1.24 (0.5)	1.52 (0.35)	

[a]Depth = 1.12 m, γ = 5/3.

[b]Values in parentheses are ratios of periods at each cover-gas pressure to those for m_f = 10 g. Variation predicted by linear theory, Eq. (16): $T \sim m_f^{0.1}$.

Table 6. Effect of depth, L[a]

Depth, L (m)	Period (ms)		
	Linear theory, Eq. (11)	Nonlinear theory, Eq. (7)	Experiment
1.12	23.0 (1.0)[b]	55 (1.0)	51.4 (1.0)
0.71		52 (0.94)	
0.20	9.89 (0.43)	29 (0.53)	36.7 (0.71)

[a]P = 0.122 MPa, m_f = 10 g, γ = 5/3. Variation predicted by linear theory, Eq. (16): $T \sim L^{1/2}$.

[b]Values in parentheses are ratios of periods at various depths to those at 1.12 m.

Table 7. Effect of γ calculated by nonlinear Eq. (7)[a]

Cover-gas pressure (MPa)	Period (ms)			
	Experiment	$\gamma = 5/3$	$\gamma = 1.4$	$\gamma = 1$
2.02	5.3 (0.14)[b]	4.4 (0.08, 0.106)	5.52 (0.04, 0.09)	9.6 (0.16, 0.06)
0.122	36.7 (1.0)	55.0 (1.0, 1.0)	61.2 (1.0, 1.0)	59.5 (1.0, 1.0)
0.025	173.9 (4.7)	128.0 (2.33, 3.55)	112.0 (1.83, 3.89)	63.2 (1.06, 4.88)

[a]Depth = 1.12 m, m_f = 10 g.

[b]Values in parentheses are ratios of periods to those at 0.122 MPa. Where two values are given, the first is that from Eq. (7) and the second is obtained from the linearized theory Eq. (11).

3.3 Application of the UVABUBL Code to FAST

Wolfgang P. Schuetz*

A number of cases were run using UVABUBL (Ref. 9) to model the water tests in the FAST Facility. On the basis of these, several changes were made in the code to improve numerical stability. Various minor changes were also made to improve readability of output and the quality of plots. In connection with the studies described in the previous sections, and with the cooperation of D. R. Bradley of the University of Virginia, the UVABUBL code was modified to include a "piston" model as well as a Rayleigh equation model in the calculation. The piston model may be used throughout, or it may be used only when the bubble has exceeded an arbitrary size. Results obtained so far are encouraging and will be presented in subsequent reports. Input data and some exploratory calculations were done for a sodium version of the FAST configuration, for CRBR conditions, and for a very large pool of sodium.

---

*Research Participant, KfK, Karlsruhe.

REFERENCES

1. T. S. Kress and J. T. Han, *LMFBR Aerosol Release and Transport Program Quart. Prog. Rep. for January–March 1979*, ORNL/NUREG/TM-329.

2. T. S. Kress and M. L. Tobias, *LMFBR Aerosol Release and Transport Program Quart. Prog. Rep. for January–March 1981*, NUREG/TM-7946.

3. T. S. Kress and M. L. Tobias, *LMFBR Aerosol Release and Transport Program Quart. Prog. Rep. for April–June 1981* (NUREG/CR-2299, Vol. 2), ORNL/TM-7974.

4. T. S. Kress and M. L. Tobias, *LMFBR Aerosol Release and Transport Program Quart. Prog. Rep. for July–September 1980* (NUREG/CR-2117), ORNL/TM-7806.

5. J. E. Smith and M. L. Jordan, "Mathematical and Graphical Interpretation of the Log-Normal Law for Particle Size Distribution Analysis," *J. Colloid Sci.* 19, 549–59 (1964).

6. R. L. Ritzman, "Examination of Solid Fission Product Plateout in Primary Systems," in *Reactor Safety Study*, Appendix VII-H, pp. 151–83, WASH-1400.

7. Nuclear Regulatory Commission, Office of Nuclear Reactor Regulations, *Technical Bases for Estimating Fission Product Behavior During LWR Accidents*, NUREG-0772, Washington, D.C. (June 1981).

8. T. S. Kress and M. L. Tobias, *LMFBR Aerosol Release and Transport Program Quart. Prog. Rep. for October–December 1980* (NUREG/CR-2215) ORNL/TM-7884.

9. D. R. Bradley, *Heat, Mass, and Momentum Transfer from Large Two-Phase Bubbles*, Ph.D. Dissertation, The University of Virginia, Charlottesville (May 1981).

NUREG/CR-2299, Vol. 3
ORNL/TM-8149
Dist. Category R7

Internal Distribution

1. R. E. Adams
2. H. W. Bertini
3. J. R. Buchanan
4. G. E. Creek
5. U. Gat
6. T. H. Hanratty (Consultant)
7. H. W. Hoffman
8-11. T. S. Kress
12. A. L. Lotts
13. R. E. MacPherson
14 A. P. Malinauskas
15. G. W. Parker
16. J. Petrykowski
17-18. T. W. Robinson, Jr.
19. J. M. Rochelle
20. R. L. Rudman (Consultant)
21. A. M. Smith
22. I. Spiewak
23. A. L. Sutton, Jr.
24. M. L. Tobias
25. H. E. Trammell
26 J. L. Wantland
27. R. P. Wichner
28. G. D. Whitman
29. A. L. Wright
30. ORNL Patent Office
31. Central Research Library
32. Document Reference Section
33-34. Laboratory Records Department
35. Laboratory Records, RC

External Distribution

36. M. Silberberg, Chief, Fuel Behavior Branch, Division of Accident Evaluation, Nuclear Regulatory Commission, Washington, DC 20555
37. R. Sherry, Division of Accident Evaluation, Nuclear Regulatory Commission, Washington, DC 20555
38-41. Director, Office of Nuclear Regulatory Research, Nuclear Regulatory Commission, Washington, DC 20555
42. Office of Assistant Manager for Energy Research and Development, DOE, Oak Ridge Operations Office, Oak Ridge, TN 37830
43. R. W. Marshall, Jr., EG&G Idaho National Engineering Laboratory P.O. Box 1625, Idaho Falls, ID 83415
44. W. A. Spencer, EG&G Idaho National Engineering Laboratory, P.O. Box 1625, Idaho Falls, ID 83415
45. R. Curtis, Chief, Severe Accident Assessment Branch, Division of Accident Evaluation, Nuclear Regulatory Commission, Washington, DC 20555
46. J. Larkins, Severe Accident Assessment Branch, Division of Accident Evaluation, Nuclear Regulatory Commission, Washington, DC 20555
47-48. Technical Information Center, DOE, Oak Ridge, TN 37830
49-343. Given distribution as shown in category R7 (NTIS-10)

*U.S. GOVERNMENT PRINTING OFFICE: 1981-546-067/367

120555051503 1 ANR7
US NRC
ADM DIV OF TIDC
PAT LARKINS
LA 212
WASHINGTON DC 20555